Fast Link Adaptation for MIMO-OFDM

Jensen, Tobias Lindstrøm; Kant, Shashi; Wehinger, Joachim; Fleury, Bernard Henri

Published in:
I E E E Transactions on Vehicular Technology

DOI (link to publication from Publisher):
10.1109/TVT.2010.2053727

Publication date:
2010

Document Version
Early version, also known as pre-print

Fast Link Adaptation for MIMO-OFDM

Tobias Lindstrøm Jensen, *Student Member, IEEE,* Shashi Kant,
Joachim Wehinger, *Member, IEEE,* and Bernard H. Fleury, *Senior Member, IEEE*

***Abstract*—We investigate link quality metrics (LQMs) based on raw bit-error-rate, effective signal-to-interference-and-noise-ratio, and mutual-information (MI) for the purpose of fast link adaptation in communication systems employing orthogonal frequency division multiplexing and multiple-input multiple-output (MIMO) antenna technology. From these LQMs the packet-error-rate (PER) can be estimated and exploited to select the modulation and coding scheme (MCS) among a class of candidate MCSs that achieves the maximum throughput for the current channel state under a specified target PER objective. We propose a novel MI-based LQM and compare the PER-estimation accuracy obtained with this LQM with that resulting from using other LQMs by means of comprehensive Monte Carlo simulations. Search methods for the MCS in the class most suitable for a given channel state are presented. An algorithm for obtaining a practical upper bound on the throughput of any link adaptation scheme is proposed. The investigated LQMs are applied to the IEEE 802.11n standard with a 2x2 MIMO configuration and practical channel estimation. The proposed MI-based LQM yields the highest PER estimation accuracy and its throughput shows only $1.7\,\mathrm{dB}$ signal-to-noise-ratio (SNR) loss with respect to the upper bound, but up to $9.5\,\mathrm{dB}$ SNR gain compared to the MCS maximizing the throughput for the current noise variance.**

***Index Terms*—Adaptive modulation and coding, link adaptation, link quality metrics, channel state information, fading, feedback delay, OFDM, MIMO, PER estimation.**

I. Introduction

The sub-carriers transmitted by a multiple-input multiple-output (MIMO) orthogonal frequency division multiplexing (OFDM) system across a time-varying frequency-selective channel are received with a quality level that varies over time, frequency and spatial streams. This knowledge can be exploited in the transmitter to adjust the modulation and coding scheme (MCS) in such a way that high-order modulations and high coding rates are used in situations of good channel state. This can be accomplished by the receiver identifying, among an indexed list of candidate MCSs, the best MCS for the current channel state and feeding the index of this MCS back to the transmitter. It was shown in, *e.g.*, [1] that adaptive modulation and coding increases the throughput of a wireless communication system tremendously. The key elements in fast link adaptation (FLA) are estimation of the packet-error-rate (PER) for different candidate MCSs and selection of the MCS that maximizes the throughput with the constraint that the time average PER lies below a specified target value. FLA also includes a time critical aspect because the selection of the best MCS for the current channel state may become obsolete as this state changes.

In systems employing MIMO OFDM antenna techniques, the main difficulty of PER estimation arises due to the unequal SNR levels in the different sub-carriers, as well as in the spatial streams when they are employed. This occurs since (i) the individual sub-carriers undergo different attenuations due to frequency selectivity and (ii) the ability of the receiver to separate multiple spatial streams depends on the condition-number of the MIMO channel matrix. The particular pattern of post-processing SINR values of the different sub-carriers induced by the channel state and the choice of the symbol detector strongly influence the decoder performance. However, the relationship between the post-processing SINR levels and the resulting bit-error-rate (BER) or PER after decoding cannot be expressed in a simple form [2]. Hence, one has to resort to a simple yet accurate mapping which provides an estimate of the PER as a function of the SINR levels.

The very same problem is of fundamental importance for system level simulations in cellular communications where the performance of a multitude of individual links are computed without actually simulating the transmission procedure of the individual bits. The latter approach would require too much computing effort to determine the overall system performance. The goal is to identify an appropriate physical layer abstraction that characterizes the instantaneous PER behaviour of the MIMO-OFDM transceiver for the current state of the time and frequency-selective channel. In UMTS-technology, based on CDMA, the assumption is that the instantaneous post-processing SINRs can be averaged (average value interface) or at least quantized using a few quantization levels [3]. This requires that the channel transfer function fades slowly versus frequency. Then the approach allows for accurate PER estimation results. However, in OFDM, multipath propagation causes a selective attenuation of the individual sub-carriers and, as a result, individual code symbols experience different SINRs. Hence, other methods have to be applied to supply reliable BER/PER estimation. One-dimensional mappings exhibit low complexity, while guaranteeing good performance [2]. An alternative is to use two-dimensional mappings that yields the PER as a function of the mean and the variance of the SINR levels [4], [5]. However, the resulting gain in accuracy is small according to [2], which shows that the gap between optimal performance and the performance achieved by one-dimensional mappings is minor. Our simulations show a similar behaviour (see Fig. 7). Thus, FLA algorithms using one dimensional mappings almost exhaust the maximal theoretical

This work was sponsored by Wipro-NewLogic Technologies, Sophia-Antipolis, France, email: wnl-info@wipro.com. Parts of this work were presented at the IEEE Int. Conf. on Communications, May 19–23, 2008, Bejing, China. T. L. Jensen and B. H. Fleury are with Dept. of Electronic Systems, Aalborg University, Denmark, email: tlj@es.aau.dk and bfl@es.aau.dk, respectively. S. Kant is with ST-Ericsson AT AB, LTE & 3G Modem Solutions, Lund, Sweden, email: shashi.kant@stericsson.com. J. Wehinger is with Infineon Technologies AG, Wireless Solutions, Neubiberg, Germany, email: j.wehinger@ieee.org.

performance improvement and the additional gain achievable by using more complex techniques is minor. This motivates the interest in one-dimensional mappings in FLA.

Robust one-dimensional mappings have been widely studied in the literature, considering methods such as uncoded BER/RawBER [6], effective SNR [7], mutual-information (MI) [8], [9] and PER indicator [10]. We propose a novel link quality metric (LQM) for MIMO-OFDM to be used for FLA. We call it mean MI bit mapping (MMIBM). We compare this metric with three other metrics, namely MI effective SNR (MIESM), effective SNR (EESM) and RawBER. We assess the estimation accuracy of all four metrics for a large number of realizations of the (frequency) transfer function of frequency-selective channels exhibiting different delay spreads. We compare the effectiveness of these metrics by realistic throughput link-level simulations including channel estimation and feedback delay. We extend the investigations in [11] by comparing further metrics, presenting a solution to problems occurring with multiple packet lengths, and addressing the important issue of how to obtain accurate mappings. In contrast to [12] we include results on the PER estimation accuracy, obtain an exact expression for the MI between the coded bits and the log-likelihood ratios (LLRs), and provide comparison among state-of-the-art PER estimation methods, as opposed to the less accurate instantaneous SNR method [2]. Furthermore, we develop a methodology to obtain an upper bound for the throughput of any link adaptation (LA) algorithm. A similar upper bound was independently proposed in [13]. However, we show that in order to obtain this bound it is only necessary to evaluate an ordered subset of the candidate MCSs instead of all candidate MCSs as done in [13]. We also prove the bound and study its tightness. In particular, we analyse the conditions for which the FLA algorithm can achieve the bound.

Notation

We denote vectors by bold lower case letters, *e.g.*, $\boldsymbol{x}$, $\boldsymbol{y}$, and matrices by bold upper case letters, *e.g.*, $\boldsymbol{H}$, $\boldsymbol{G}$. The conjugate transpose of the matrix $\boldsymbol{A}$ is denoted by $\boldsymbol{A}^{\mathrm{H}}$. The element in the i-th row and j-th column of $\boldsymbol{A}$ is denoted as $[\boldsymbol{A}]_{i,j}$. The $Q \times Q$ identity matrix is written as $\boldsymbol{I}_Q$. The expectation operator is denoted by $\mathbb{E}\{\cdot\}$ and $\mathbb{C}$ is the set of complex numbers.

II. System Model

We choose the IEEE 802.11n standard as a concrete example for the system model. However, other systems, like IEEE 802.16d/e or 3GPP-LTE, can be described in a similar way. The setup common to these systems is depicted in Fig. 1. This figure shows the simplified block diagram of a MIMO bit-interleaved coded modulation (BICM) OFDM system equipped with N_{T} transmit antennas and N_{R} receive antennas. In the IEEE 802.11n system, the information bit stream $\{b\}$ is encoded using a convolutional encoder with generators $[133, 171]$ in octal representation and basic code rate $R_c = 1/2$. The coded bit stream may be punctured to increase the code rate to $2/3$, $3/4$ or $5/6$, depending on the used MCS. The stream of interleaved and spatially parsed bits is mapped to a stream of complex symbols using Gray mapping. Supported sub-carrier modulation formats are BPSK, QPSK, 16QAM and 64QAM. The candidate MCSs available are enumerated according to a certain order. In the sequel, Ω denotes the index set of the MCSs in this list. By convention, the term MCS might designate either the MCS scheme itself or its index in Ω. The available MCSs for single-stream and dual-stream transmission are listed with their index in Table I. Their maximum throughput is reported in the columns "Throughput". BICM schemes using different coding and modulation per stream in multi-stream transmission are given in [14].

The streams of complex symbols $\{x\}$ are modulated in an OFDM format with $N_{\mathrm{SD}} = 52$ data sub-carriers of $312.5\,\mathrm{kHz}$ bandwidth. The total bandwidth of the OFDM signal is $20\,\mathrm{MHz}$. The relationship for the k-th sub-carrier, $k = 1, \ldots, N_{\mathrm{SD}}$, between the input of the spatial expansion scheme and the output of the OFDM receiver in Fig. 1 is

$$\boldsymbol{y}[k] = \boldsymbol{H}[k]\boldsymbol{x}[k] + \boldsymbol{n}[k]\,, \tag{1}$$

where $\boldsymbol{y}[k] \in \mathbb{C}^{N_{\mathrm{R}}}$ and $\boldsymbol{x}[k] \in \mathbb{C}^{N_{\mathrm{SS}}}$ are the received signal vector and the transmitted symbol vector respectively for sub-carrier k and $\boldsymbol{n}[k] \in \mathbb{C}^{N_{\mathrm{R}}}$ is a complex zero-mean Gaussian noise vector with covariance matrix $\sigma_n^2 \boldsymbol{I}_{N_{\mathrm{R}}}$. The variable N_{SS} denotes the number of spatial streams and $\boldsymbol{H}[k] \in \mathbb{C}^{N_{\mathrm{R}} \times N_{\mathrm{SS}}}$ describes the effective channel matrix, including the channel transfer function, the cyclic delay diversity (CDD) and the spatial expansion [14] for sub-carrier k. Spatial expansion transmits N_{SS} symbol streams over N_{T} transmit antennas, where $N_{\mathrm{SS}} \leq N_{\mathrm{T}}$. When spatial multiplexing is employed, $N_{\mathrm{SS}} = N_{\mathrm{T}}$. When either beamforming or Alamouti space-time coding is applied, $N_{\mathrm{SS}} < N_{\mathrm{T}}$. The CDD transmits a cyclicly delayed OFDM symbol waveform through each transmit antenna in order to obtain frequency diversity at the receiver side.

An unbiased linear minimum mean square error (MMSE) estimator is used to recover the transmitted symbol from the received signal $\boldsymbol{y}[k]$:

$$\hat{\boldsymbol{x}}[k] = \boldsymbol{G}^{\mathrm{H}}[k]\boldsymbol{y}[k]\,. \tag{2}$$

The $N_{\mathrm{R}} \times N_{\mathrm{SS}}$ matrix $\boldsymbol{G}[k] = \Big[\boldsymbol{G}_1[k], \boldsymbol{G}_2[k], \ldots, \boldsymbol{G}_{N_{\mathrm{SS}}}[k]\Big]$ has columns given by

$$\begin{aligned}\boldsymbol{G}_j[k] = \frac{1}{\boldsymbol{H}_j^{\mathrm{H}}[k]\left(\boldsymbol{H}[k]\boldsymbol{H}^{\mathrm{H}}[k] + \sigma_n^2\boldsymbol{I}_{N_{\mathrm{R}}}\right)^{-1}\boldsymbol{H}_j[k]} \\ \cdot \left(\boldsymbol{H}[k]\boldsymbol{H}^{\mathrm{H}}[k] + \sigma_n^2\boldsymbol{I}_{N_{\mathrm{R}}}\right)^{-1}\boldsymbol{H}_j[k]\,,\end{aligned} \tag{3}$$

$j = 1, 2, \ldots, N_{\mathrm{SS}}$, with $\boldsymbol{H}_j[k]$ denoting the columns of $\boldsymbol{H}[k]$, *i.e.*, $\boldsymbol{H}[k] = [\boldsymbol{H}_1[k], \boldsymbol{H}_2[k], \ldots, \boldsymbol{H}_{N_{\mathrm{SS}}}[k]\,]$. Notice that the linear biased MIMO-MMSE corresponds to (3) with the expression in the denominator set to one. The post-processing signal-to-interference-and-noise ratio (SINR) at the output of the linear MMSE estimator for the j-th stream and k-th tone is given by [15]

$$\gamma_j[k] = \frac{1}{\left[\left(\frac{E_{\mathrm{s}}}{\sigma_n^2 N_{\mathrm{T}}}\boldsymbol{H}^{\mathrm{H}}[k]\boldsymbol{H}[k] + \boldsymbol{I}_{N_{\mathrm{SS}}}\right)^{-1}\right]_{j,j}} - 1\,, \tag{4}$$

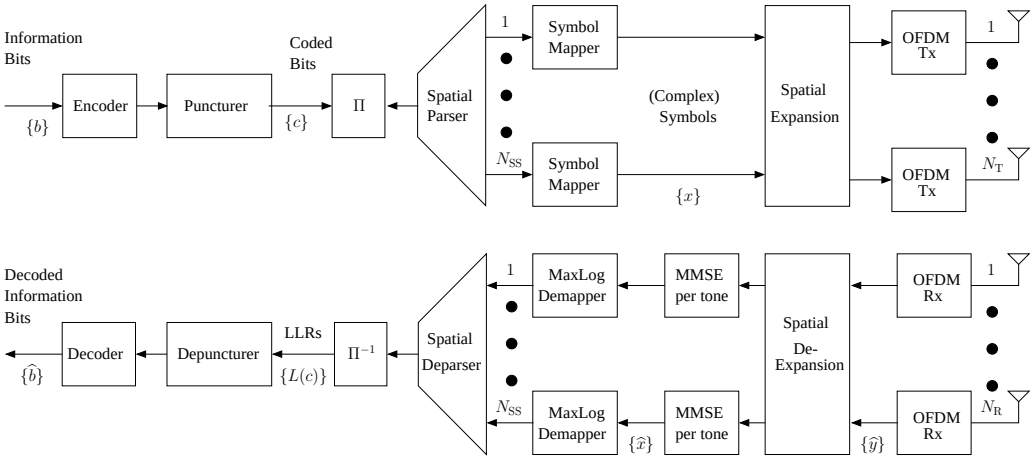

Fig. 1. Block diagram of a MIMO-OFDM system employing BICM.

TABLE I
MCSs WITH THEIR INDICES AND ACHIEVABLE THROUGHPUTS FOR SINGLE-STREAM AND DOUBLE-STREAM (IN PARENTHESES) TRANSMISSION WITH EQUAL SUB-CARRIER MODULATION. AN 800 ns GUARD INTERVAL IS USED IN IEEE 802.11n [14].

Index m	Sub-carrier modulation	R_c	Throughput [Mbps]	Index m	Sub-carrier modulation	R_c	Throughput [Mbps]
0 (8)	BPSK	1/2	6.5 (13.0)	4 (12)	16QAM	3/4	39.0 (78.0)
1 (9)	QPSK	1/2	13.0 (26.0)	5 (13)	64QAM	2/3	52.0 (104.0)
2 (10)	QPSK	3/4	19.5 (39.0)	6 (14)	64QAM	3/4	58.5 (117.5)
3 (11)	16QAM	1/2	26.0 (52.0)	7 (15)	64QAM	5/6	65.0 (130.0)

$k = 1, 2, \ldots, N_{\mathrm{SD}}$, $j = 1, 2, \ldots, N_{\mathrm{SS}}$, with $E_{\mathrm{s}}/\sigma_n^2$ denoting the SNR measured at the ports of each receive antenna. A MaxLog symbol demapper is used to generate log-likelihood ratios (LLRs) for the coded bits, which are then multiplexed into a single stream $\{L(c)\}$. This stream is de-interleaved and de-punctured before it is fed to a Viterbi decoder that computes the information bit estimates $\{\hat{b}\}$. In this paper we focus on the case with $N_{\mathrm{T}} = N_{\mathrm{R}} = 2$ antennas. The IEEE Channel Model B (root mean square (RMS) delay spread $15\,\mathrm{ns}$, excess delay spread $80\,\mathrm{ns}$) and Channel Model E (RMS delay spread $100\,\mathrm{ns}$, excess delay spread $730\,\mathrm{ns}$) with $20\,\mathrm{MHz}$ system-bandwidth are used [16].

III. FAST LINK ADAPTATION

The objective of FLA is to exploit the varying channel state to increase the throughput of the system, while maintaining some target PER (PER_{target}). The FLA algorithm employed in the receiver feeds the index of the selected MCS back to the transmitter. This MCS feedback (MFB) response may occur based upon request from the transmitter.

The FLA algorithm considers the channel state information via the post-processing SINRs of all spatial streams and sub-carriers $\mathbf{\Gamma} = \left[\gamma_j[k]\right]_{j=1,\ldots,N_{\mathrm{SS}};\ k=1,\ldots,N_{\mathrm{SD}}}$. For a given MCS m, the FLA algorithm computes a scalar LQM value $q = q(m;\mathbf{\Gamma})$. The PER value $PER_{m,p}(\mathbf{\Gamma})$ for packet length p corresponding to the current realization of the channel transfer function is estimated by $PER_{m,p}^{\mathrm{AWGN}}(q)$, *i.e.*, the PER achieved when the MCS transmits across the AWGN channel with quality metric q. The latter mapping circumvents the need to store a look-up table of $PER_{m,p}(\mathbf{\Gamma})$ functions for some selected (quantized) SINR matrices. Indeed, the set of such quantized matrices required is large, which makes an implementation of this approach problematic.

Thus, for a given MCS m transmitting packets of length p across a channel inducing post-processing SINRs $\mathbf{\Gamma}$, the LQM-to-PER mapping is determined such that the approximations

$$PER_{m,p}(\mathbf{\Gamma}) \approx PER_{m,p}^{\mathrm{AWGN}}(q(m;\mathbf{\Gamma})) \approx \psi_{m,p}(q(m;\mathbf{\Gamma})) \quad (5)$$

hold. For each MCS $m \in \Omega$ and packet length p of interest, the function $\psi_{m,p}(q)$ is computed considering two different channel quality metric, namely the SNR γ and the MI $\mathcal{I}$ of the AWGN channel. Each function is obtained by fitting a quadratic log-linear regression to a set of $\left(q, PER_{m,p}^{AWGN}\right)$ pairs $(q \in \{\gamma, \mathcal{I}\})$ obtained from Monte Carlo simulations. The PER performances of the single-stream MCSs reported in Table I are depicted in Fig. 2 and Fig. 3 versus γ and $\mathcal{I}$ respectively together with the approximation functions $\psi_{m,p_{\mathrm{ref}}}(\gamma)$ and $\psi_{m,p_{\mathrm{ref}}}(\mathcal{I})$ respectively where a reference packet length $p_{\mathrm{ref}} = 1024\,\mathrm{Bytes}$ is considered. As can be seen from these figures the fit provided by $\psi_{m,p_{\mathrm{ref}}}(q)$ to the simulation results is good. Closer inspection of Fig. 2 reveals that a single dB change in γ leads to a PER change of up to 1.5 decade. The same comment applies to the PER performance versus $\mathcal{I}$ reported in Fig. 3. This implies that the LQM function $q(m, \Gamma)$ must be very accurate. In Section IV we will consider different SNR- and MI-based LQMs that will be used as arguments of respectively $\psi_{m,p}(\gamma)$ and $\psi_{m,p}(\mathcal{I})$ to estimate the PER. We will assess the accuracy of these LQMs in Section V.

IV. LINK QUALITY METRICS

In this section, we define the four investigated LQMs. The first two LQMs are based on the concept of MI. The third LQM relies on a weighting of the entries in $\mathbf{\Gamma}$ in a log-sum-exp manner. The last LQM is based on raw BER. The MI-based LQMs basically compute the mean MI (MMI) per sub-carrier symbol in the receiver, where the MI of one symbol is obtained by averaging the MIs of the bits mapped in this

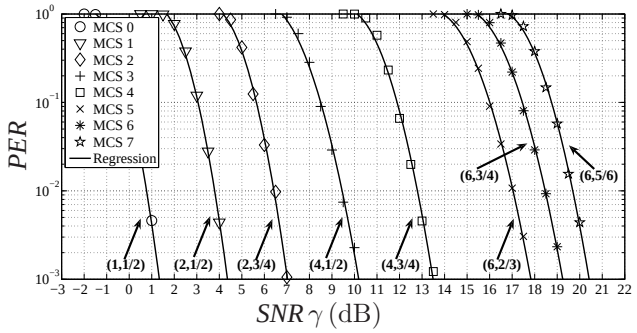

Fig. 2. PER versus SNR in the AWGN channel of the MCSs in Table I with packet length $p_{\mathrm{ref}} = 1024$ Bytes computed from Monte Carlo simulations. The functions $\psi_{m,p_{\mathrm{ref}}}(\gamma)$ (solid lines) are obtained by fitting a quadratic log-linear regression to the simulation results.

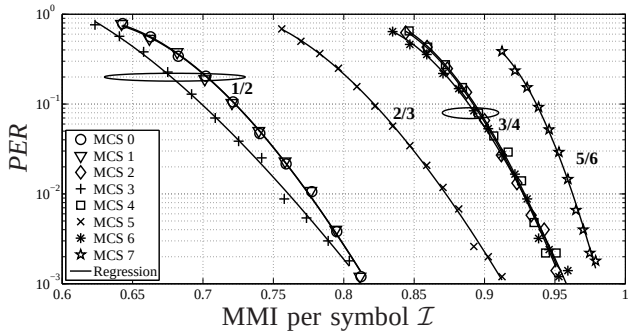

Fig. 3. PER versus MMI per symbol in the AWGN channel of the MCSs in Table I with packet length $p_{\mathrm{ref}} = 1024$ Bytes computed from Monte Carlo simulations. The functions $\psi_{m,p_{\mathrm{ref}}}(\mathcal{I})$ (solid lines) are obtained by fitting a quadratic log-linear regression to the simulation results. PER curves corresponding to the same code-rate are bundled with an ellipse.

symbol [8]. This LQM corresponds to the mean MI between the stream of coded bits $\{c\}$ at the output of the puncturer in the transmitter and the corresponding stream of LLRs $\{L(c)\}$ at the output of the de-interleaver in the receiver (see Fig. 1). The accuracy of the four investigated LQMs is assessed in two types of frequency-selective channels in the next section.

A. Mean Mutual Information per Coded Bit Mapping (MMIBM)

MI-based metrics are used in system-level simulations to estimate the PER since they achieve a high PER estimation accuracy for a large variety of realizations of the channel transfer function [4], [9], [17]. In [8], an MI-based LQM is suggested for system-level simulations in IEEE 802.16e. This metric computes the effective MMI per (sub-carrier) symbol

$$\mathcal{I}'_{\mathrm{eff}}(m;\mathbf{\Gamma}) = \frac{1}{N_{\mathrm{SS}}N_{\mathrm{SD}}}\sum_{j=1}^{N_{\mathrm{SS}}}\sum_{k=1}^{N_{\mathrm{SD}}}\mathcal{I}_{M(m)}\left(\gamma_j[k]\right). \quad (6)$$

The PER is estimated by inserting $\mathcal{I} = \mathcal{I}'_{\mathrm{eff}}(m;\mathbf{\Gamma})$ in the corresponding function $\psi_{m,p}(\mathcal{I})$ depicted in Fig. 3. The function $\mathcal{I}_M(\gamma)$ in (6) is the MI per symbol for the modulation format M at SNR γ. The function $M(m)$ specifies the modulation format of MCS m. For the MaxLog demapper under consideration $\mathcal{I}_M(\gamma)$ is selected as follows:

$$\mathcal{I}_M(\gamma)\begin{cases} = J\left(\sqrt{8\gamma}\right) & ;\ M = \text{BPSK} \\ = J\left(\sqrt{4\gamma}\right) & ;\ M = \text{QPSK} \\ \approx \frac{1}{2}J\left(0.8818\sqrt{\gamma}\right) + \frac{1}{4}J\left(1.6764\sqrt{\gamma}\right) & \\ \quad + \frac{1}{4}J\left(0.9316\sqrt{\gamma}\right) & ;\ M = \text{16QAM} \\ \approx \frac{1}{3}J\left(1.1233\sqrt{\gamma}\right) + \frac{1}{3}J\left(0.4381\sqrt{\gamma}\right) & \\ \quad + \frac{1}{3}J\left(0.4765\sqrt{\gamma}\right) & ;\ M = \text{64QAM} \end{cases}. \quad (7)$$

The function $J(\cdot)$ is given in (25) in Appendix C. Assuming an equivalent Gaussian channel for each sub-carrier after MMSE equalization [18], $\mathcal{I}_M(\gamma)$ is given in closed form as a function of the SNR γ for $M =$ BPSK and $M =$ QPSK [8]. No closed-form expression for $\mathcal{I}_M(\gamma)$ is known for the high-order modulation formats $M =$ 16QAM and $M =$ 64QAM. In [8], $\mathcal{I}_{16\mathrm{QAM}}(\gamma)$ and $\mathcal{I}_{64\mathrm{QAM}}(\gamma)$ are approximated by numerical integration of the LLR histogram. These relations are then approximated with the linear combinations of expanded/compressed versions of $J(\gamma)$ given in (7). We propose a simple and more elegant method to derive an approximation of $\mathcal{I}_{16\mathrm{QAM}}(\gamma)$ and $\mathcal{I}_{64\mathrm{QAM}}(\gamma)$. The method computes first the MMI using the reliability of the LLRs along [19]:

$$\mathcal{I}_{\mathrm{LLR}}(\mathbf{L}) = \left(\frac{1}{N_{\mathrm{symb}}N_{\mathrm{SS}}N_{\mathrm{SD}}N_{\mathrm{bits}}}\right) \cdot \sum_{n=1}^{N_{\mathrm{symb}}}\sum_{j=1}^{N_{\mathrm{SS}}}\sum_{k=1}^{N_{\mathrm{SD}}}\sum_{i=1}^{N_{\mathrm{bits}}} f\left(\left|L_j^n[k](c_i)\right|\right). \quad (8)$$

In this expression, N_{symb} is the number of OFDM symbols, N_{bits} is the number of bits mapped to one sub-carrier symbol, $L_j^n[k](c_i)$ is the LLR of the i-th coded bit in the n-th OFDM symbol for sub-carrier k of the j-th spatial stream, and $\mathbf{L} = \left[L_j^n[k](c_i)\right]_{j=1,\ldots,N_{\mathrm{SS}};k=1,\ldots,N_{\mathrm{SD}};i=1,\ldots,N_{\mathrm{bits}};n=1,\ldots,N_{\mathrm{symb}}}$. The function $f(\cdot)$ is given by [19]

$$f(x) = \left(\frac{1}{1+\exp(+x)}\right)\log_2\left(\frac{2}{1+\exp(+x)}\right) + \left(\frac{1}{1+\exp(-x)}\right)\log_2\left(\frac{2}{1+\exp(-x)}\right),\ x \geq 0. \quad (9)$$

Sets of $\mathcal{I}_{\mathrm{LLR}}(\mathbf{L})$ are computed for 16QAM and 64QAM signaling across the AWGN channel for a wide range of the SNR γ. Then non-linear least-squares fits (cf. [20]) are performed to these sets to obtain the coefficients of the approximations for $\mathcal{I}_{16\mathrm{QAM}}(\gamma)$ and $\mathcal{I}_{64\mathrm{QAM}}(\gamma)$ in (7). Notice that the MMI in (8) is not used as an LQM in this paper. It is merely employed to compute the approximations in (7).

The MMI per symbol in (6) is used to estimate the PER of MCSs operating in fading channels [8]. However, simulations show that the MMI per symbol does not accurately estimate the PER in IEEE 802.11n fading channels due to the high dynamic of the MI per symbol (or of the entries in $\mathbf{\Gamma}$) due to frequency selectivity. As a remedy, in [13] the authors propose to replace the sum in (6) by a weighted sum of first-order statistics. Inspired by [21], we propose an alternative approach

in which the right-hand side of (6) is augmented with a term that reflects this dynamic:

$$\mathcal{I}_{\text{eff}}\left(m;\mathbf{\Gamma}\right) = \frac{1}{N_{\text{SS}}N_{\text{SD}}}\sum_{j=1}^{N_{\text{SS}}}\sum_{k=1}^{N_{\text{SD}}}\mathcal{I}_{M(m)}\Big(\gamma_j[k]\Big) + \lambda(m)\left[\frac{1}{N_{\text{SS}}}\sum_{j=1}^{N_{\text{SS}}}\text{var}_k\Big\{\mathcal{I}_{M(m)}\Big(\gamma_j[k]\Big)\Big\}\right]. \quad (10)$$

In this expression $\text{var}_k\{x\}$ is the sample variance of x computed versus the index k. The motivation for including the correction term is as follows. We know that high frequency selectivity decreases the PER, *i.e.*, leads to a higher $\mathcal{I}_{\text{eff}}$. Channel coding across sub-carriers is indeed able to compensate for sub-carriers with low MI per symbol when the frequency transfer function of the channel significantly fluctuates over the ODFM bandwidth. As a result the PER performance is lower than that obtained from the MMI per symbol in (6). The term in the brackets in (10) is used as a measure of the fluctuation of the channel transfer function across the sub-carriers. It is obtained by first computing for each stream the variance of the MIs of the subcarriers and then taking the average of the MI variances of all streams. Note that this approach using $\mathcal{I}_{\text{eff}}$ in (10) is different from the one proposed in [13] where (6) is replaced by a weighted sum of MI per symbol values. The correction term in (10) considers an estimate of the variance of these values, while in [13] these values are individually weighted.

The parameter $\lambda(m)$ balances the contribution of the MI mean and variance terms in $\mathcal{I}_{\text{eff}}$. It is calibrated for each MCS individually by performing a least-squares fit in the $\log(\mathit{PER})$-domain [17]:

$$\lambda(m) = \underset{\lambda}{\text{argmin}}\left\{\sum_{i=1}^{N}\left|e_m^{(i)}(\lambda)\right|^2\right\}, \quad (11)$$

where $e_m^{(i)}(\lambda) = \log\Big(\psi_{m,p}(q^{(i)}(\lambda))\Big) - \log\Big(\mathit{PER}_{m,p}^{(i)}\Big)$. The parameter N is the number of considered realizations of the channel transfer function, $\mathit{PER}_{m,p}^{(i)}$ is the simulated PER for MCS m, the ith transfer function realization and a given noise variance, while $\psi_{m,p}(q^{(i)}(\lambda))$ is the corresponding estimated PER for the given selection of λ. To calibrate $\lambda(m)$ for a given MCS m it is necessary to consider a sufficiently large number of independent realizations of the channel transfer function [2]. For each MCS m we calibrate $\lambda(m)$ by considering in total 45-50 realizations of the transfer function generated with both Channel Model B and Channel Model E. Even though the calibration is conducted based on realizations drawn with both models, the accuracy of the resulting PER estimator is still accurate when the realizations are generated with one of the two models only. This supports the thesis that the FLA does not need to know the prevailing channel type. The proposed calibration approach is consistent with the method used in [2], [22]. Other PER estimation techniques show similar results [23], [24].

As shown in Fig. 4, the introduction of the additional term in (10) with $\lambda(m)$ selected according to (11) significantly reduces the mean-square error (MSE)

$$\text{MSE}(m) = \frac{1}{N}\sum_{i=1}^{N}\left|e_m^{(i)}(\lambda(m))\right|^2. \quad (12)$$

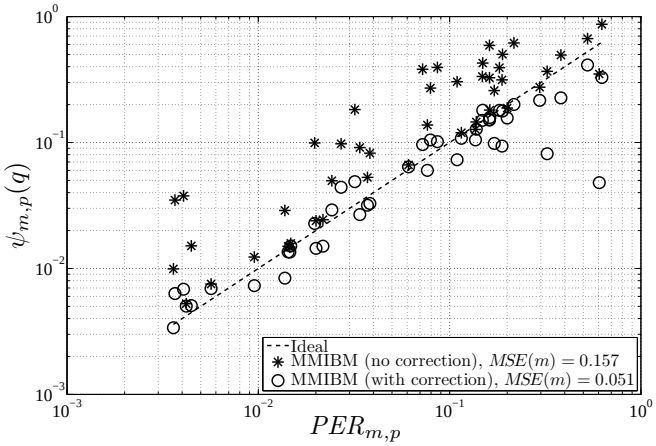

Fig. 4. Estimated PER $\psi_{m,p}(q)$ versus computed $\mathit{PER}_{m,p}$ without and with correction parameter for $m = 0$ (BPSK, $R_{\text{c}} = 1/2, p = 1024\,\text{Bytes}$), SISO system, Channel Model B and Channel Model E. One depicted point corresponds to one realization of the channel transfer function. The resulting MSEs are also reported in the legend. One data set is used both for calculating the correction parameters and computing the estimated PER values.

B. Mutual Information Effective SNR Mapping (MIESM)

The second metric is an effective SNR based on MI proposed in [17]:

$$\gamma_{\text{eff}}(m;\mathbf{\Gamma}) = \kappa(m)\left[J^{-1}\left(\frac{1}{N_{\text{SS}}N_{\text{SD}}}\sum_{j=1}^{N_{\text{SS}}}\sum_{k=1}^{N_{\text{SD}}}J\left(\sqrt{\frac{\gamma_j[k]}{\kappa(m)}}\right)\right)\right]^2. \quad (13)$$

The functions $J(y)$ and $J^{-1}(y)$ are given in (25) and (26) respectively in Appendix C. The parameter $\kappa(m)$ is calibrated with the same method as used to obtain $\lambda(m)$ (see (11)). For the special case of BPSK a modified version was already given in [9]. The PER is estimated by inserting $\gamma = \gamma_{\text{eff}}(m;\mathbf{\Gamma})$ in the corresponding function $\psi_{m,p}(\gamma)$ depicted in Fig. 2.

C. Exponential Effective SNR Mapping (EESM)

The third considered metric is the effective SNR proposed in [7] [25]. The metric is defined for a given MCS m to be

$$\gamma'_{\text{eff}}(m;\mathbf{\Gamma}) = -\beta(m)\log\left(\frac{1}{N_{\text{SS}}\,N_{\text{SD}}}\sum_{j=1}^{N_{\text{SS}}}\sum_{k=1}^{N_{\text{SD}}}\exp\left(-\frac{\gamma_j[k]}{\beta(m)}\right)\right). \quad (14)$$

The parameter $\beta(m)$ is calibrated with the same method as used to obtain $\lambda(m)$. The PER is estimated by inserting $\gamma = \gamma'_{\text{eff}}(m;\mathbf{\Gamma})$ in the corresponding function $\psi_{m,p}(\gamma)$ depicted in Fig. 2.

D. Raw Bit-Error-Rate (RawBER)

This mapping computes a single scalar value by averaging the uncoded bit-error rates of all sub-carriers [6] [26]:

$$\mathit{RawBER}'(m;\mathbf{\Gamma}) = \frac{1}{N_{\mathrm{SS}}\,N_{\mathrm{SD}}}\sum_{j=1}^{N_{\mathrm{SS}}}\sum_{k=1}^{N_{\mathrm{SD}}}\mathit{RawBER}_{j,M(m)}[k]\,. \tag{15}$$

In the right-hand expression $\mathit{RawBER}_{j,M}[k]$ is the raw BER of the jth spatial stream and kth sub-carrier when using the modulation format M. A function $\psi_{m,p}(\mathit{RawBER})$ is used as an estimate of the PER. Let us for example consider the modulation format $M = \text{BPSK}$. If we assume that the output of the MMSE receiver can be approximated as the output of an AWGN channel [18], we have

$$\mathit{RawBER}_{j,\mathrm{BPSK}}[k] \approx Q\left(\sqrt{2\,\gamma_j[k]}\right). \tag{16}$$

Notice that this metric is independent of the used code. We introduce a correction similar to that applied to EESM (see (14)) for RawBER:

$$\mathit{RawBER}(m;\mathbf{\Gamma}) = \left(\frac{1}{N_{\mathrm{SS}}\,N_{\mathrm{SD}}}\sum_{j=1}^{N_{\mathrm{SS}}}\sum_{k=1}^{N_{\mathrm{SD}}}Q\left(\sqrt{\frac{2\,\gamma_j[k]}{\alpha(m)}}\right)\right)^{\sqrt{\alpha(m)}}. \tag{17}$$

The parameter $\alpha(m)$ is calibrated with the same method as used to obtain $\lambda(m)$. The method can be generalized to arbitrary subcarrier modulation formats. Simulations show that with this correction, the accuracy of the PER estimation increases.

V. Accuracy of the PER Estimates

In this section, we discuss the PER estimation accuracy of the four considered LQMs. The accuracy of the approximation in (5) can be assessed numerically by Monte Carlo simulations. To this end, estimates of the left-hand term $\left(\mathit{PER}_{m,p}(\mathbf{\Gamma})\right)$ and the right-hand term $\left(\psi_{m,p}\left(q(m;\Gamma)\right)\right)$ in (5) for a particular LQM q are computed for various realizations of the channel transfer function. The steepness of the function $\mathit{PER}_{m,p}^{\mathrm{AWGN}}(q)$ requires the calculated LQMs to be quite accurate. An inaccuracy of $1\,\mathrm{dB}$ can lead to a PER estimate shifted 1.5 decades away from the true PER. Fig. 5 shows a scatter plot of pairs of computed and estimated PERs using the considered LQMs for different realizations of the channel transfer function generated with the Channel Model B and Channel Model E. Table II reports the correction parameters for these LQMs. The values are given in dB with $(\cdot)_{\mathrm{dB}} = 20\,\log_{10}(\cdot)$.

It can be seen that the MMIBM, MIESM and EESM metrics provide nearly the same PER estimation accuracy, with MMIBM slightly outperforming the other two metrics. The RawBER metric shows the largest MSE. We observe outliers which result when the interleaving depth of the interleaver is mismatched to the current channel state. Indeed, a static interleaver, as used in IEEE 802.11n [14], is designed according to average channel statistics, *i.e.*, the coherence bandwidth and coherence time. However, individual realizations of the channel transfer function may exhibit an instantaneous coherence bandwidth and/or coherence time exceeding the interleaver depth. In this case all soft bits at the interleaver output will be affected by similar highly correlated channel weights [27]. This, motivates the use of adaptive interleavers [28]. Even with the presence of the outliers, the scatter plots in Fig. 5 show that the correction parameters are valid for both Channel Model B and Channel Model E. We observed that each correction parameter is robust, *i.e.*, a small variation of it results in a small variation of the PER estimates.

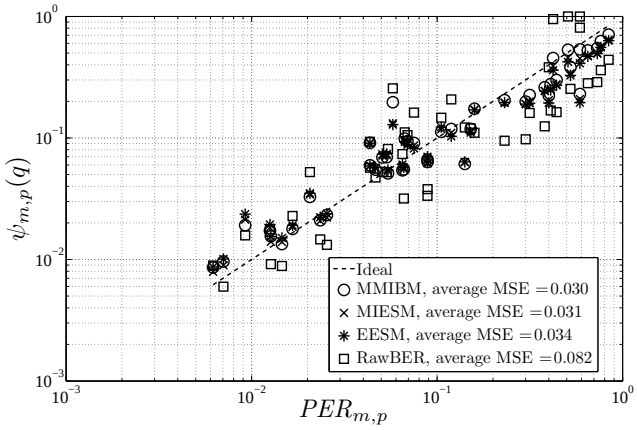

(a) $m \in \{3, 11\}$

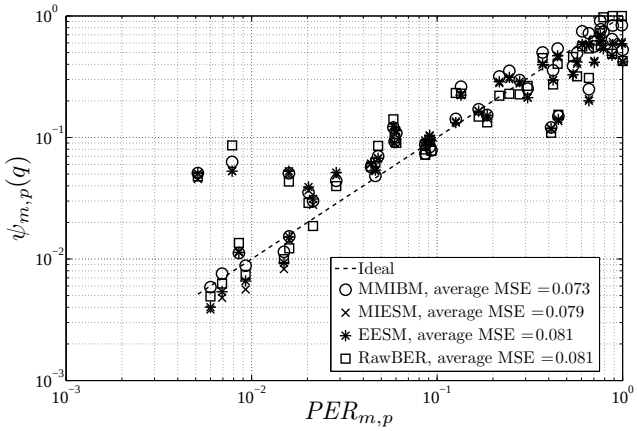

(b) $m \in \{7, 15\}$

Fig. 5. Scatter plots of estimated PER $\psi_{m,p}(q)$ versus computed $\mathit{PER}_{m,p}$ for MCSs with same modulation and coding per stream $m \in \{3, 11\}$ (a) and $m \in \{7, 15\}$ (b). The data points are joined from both MCSs. The data are obtained for realizations of the channel transfer functions generated with Channel Model B (2×2 MIMO) and Channel Model E (SISO) using a packet length $p = 1024\,\mathrm{Bytes}$. The respective correction parameters of the LQMs are computed from these scatter plots. The average MSEs are also reported in the legends, ex: $\frac{1}{2}(\mathrm{MSE}(3) + \mathrm{MSE}(11))$. One data set is used both for finding the correction parameters and computing the estimated PER values.

VI. Mapping of the Estimated PER Versus Packet Length

The function $\psi_{m,p}(q)$ is parameterized by the MCS index m and packet length p. It should therefore be computed for each pair (m, p), $m \in \Omega$ and p ranging in the set of supported packet lengths. However, in order to keep the complexity of the mapping low, it is desirable to store $\psi_{m,p}(q)$ for a few of the most used packet length values only and to interpolate the

TABLE II
CORRECTION PARAMETERS OF THE LQMS COMPUTED CHANNEL MODEL B AND CHANNEL MODEL E. ALL VALUES ARE IN dB.

MCS Index	0 (8)	1 (9)	2 (10)	3 (11)	4 (12)	5 (13)	6 (14)	7 (15)
$\alpha(m)$	2.61	2.70	2.66	1.22	1.74	0.99	1.22	1.42
$\beta(m)$	0.13	3.15	3.12	8.52	9.45	14.68	15.34	15.70
$\kappa(m)$	7.80	4.77	5.08	-0.60	-1.28	-6.62	-7.19	-7.51
$\lambda(m)$	-3.89	-4.15	-2.64	-5.97	-4.23	-5.21	-3.79	-2.48

PER for other packet length values from this set of reference functions. The simple case, which we consider here, is when the set contains one element $\psi_{m,p_{\mathrm{ref}}}(q)$ only. We propose the following interpolation:

$$\psi_{m,p}(q) = 1 - \left(1 - \psi_{m,p_{\mathrm{ref}}}(q)\right)^{\frac{p}{p_{\mathrm{ref}}}}. \tag{18}$$

The right-hand expression yields a reasonable approximation across a wide range of p. This approximation has, however, a limitation: $\psi_{m,p}(q) = 1$ for all p when $\psi_{m,p_{\mathrm{ref}}}(q) = 1$. If a higher accuracy is needed, multiple reference curves can be used. Since the set of packet lengths supported in a practical network is small, storing multiple reference curves is a minor practical problem. The approach presented in [29] is an attractive alternative for turbo-codes.

VII. MCS SEARCH

The selected MCS fed back to the Tx is the MCS keeping the PER below a given threshold, PER_{th}. This selection procedure leads to a discrete optimization problem that can be formulated as

$$\begin{aligned} \max_{m\in\Omega} \quad & TP(m) \\ \text{s.t.} \quad & \psi_{m,p}(q(m;\mathbf{\Gamma})) \leq PER_{\mathrm{th}}\,, \forall m \in \Omega \Big\backslash \left\{ \operatorname*{argmin}_{m\in\Omega} TP(m) \right\} \end{aligned} \tag{19}$$

for the prevailing SINR matrix $\mathbf{\Gamma}$. In (19), PER_{th} is selected such that PER_{target} is met on average over time. This step includes some heuristics and is based on experimental evidence. The parameter PER_{target} essentially controls the delay/jitter of the link, if retransmission is needed, and of course the throughput. Different PER_{target} can therefore be used according to the quality of service needed for the considered applications (digital video streaming, voice over IP, web-browsing, etc.).

Note that at sufficiently high and low SNR regimes it is not possible to obtain a PER close to PER_{target}. This is because transmission with all MCSs will almost always succeed at sufficiently high SNR, while it will almost always fail at sufficiently low SNR. If at an given mid SNR regime PER_{th} is selected such that PER_{target} is fulfilled on average, this PER might not be reached within a small time window. The following algorithm controls PER_{th} such that the FLA algorithm approximately delivers a given PER_{target} within a certain time window: If the recorded PER is too high or too low as time elapses in the window, then adjust PER_{th} such that PER is approximately equal to PER_{target} at the end of the window.

It is desired that the Rx always feeds back an MCS index to the Tx. Excluding the MCS with the lowest throughput in the constraints of the optimization problem (19) guarantees that this problem always has a solution. If no MCS succeeds in providing a sufficiently small PER, a situation that occurs at sufficiently low SNR, the Rx feeds back $m = \operatorname{argmin}_{m\in\Omega} TP(m)$ to the Tx.

In the literature either the objective function $TP(m)$ in (19) or $(1 - \psi_{m,p}(q(m;\mathbf{\Gamma})))TP(m)$ is used for selecting the MCS to be utilized, see *e.g.*, [13], [30]. The two objective functions are equivalent if

$$PER_{\mathrm{th}} < \min_{m_1,m_2} \left\{ 1 - \frac{TP(m_1)}{TP(m_2)} \right\} \tag{20}$$

where

$$m_1, m_2 \in \Omega, m_1 \neq m_2 \text{ such that } TP(m_1) \leq TP(m_2)\,,$$

since $TP(m)$ cannot differ from $(1-\psi_{m,p}(q(m;\mathbf{\Gamma})))TP(m)$ by more than a factor $1 - PER_{\mathrm{th}}$ because of the PER constraints in (19). Condition (20) is fulfilled in the simulation setup provided in Section IX. Hence, the MCS selection algorithm is optimal with respect to both the objective function $TP(m)$ and $(1 - \psi_{m,p}(q(m;\mathbf{\Gamma})))TP(m)$ for these simulations.

One way of solving (19) is by performing an exhaustive search across all elements in Ω [13]. We propose a sequential search, in which the MCSs are first ordered in decreasing order of their throughput and then the PER of each MCS in the list is evaluated one by one. The first MCS that fulfils the PER constraint in (19) is the sought solution, because it has the maximum throughput among the MCS satisfying the PER constraint, due to the selected ordering. Both exhaustive and sequential search procedures lead to the same solution. However, the sequential search method has a smaller computational burden compared to the exhaustive search method. For instance the latter approach searches in the complete set of cardinality 16 for $N_{\mathrm{T}} = 2$ [14] when the same modulation format is used on both spatial streams, while the former stops earlier in general. Both methods are applicable when the number of candidate MCSs, *i.e.*, the cardinality of Ω, is fairly low. We apply the sequential search method to assess the performance of the FLA algorithms in Section IX.

In case unequal modulation formats are used in the spatial streams, the effective MI is computed to be a weighted sum of the mutual information values calculated for the individual streams. The weights equal the relative fractions of information bits transmitted in the streams.

The transmission mode can use beamforming or spatial-multiplexing depending on the condition-number of the channel. This would, for example, imply $N_{\mathrm{SS}} = 1$ for beamforming and $N_{\mathrm{SS}} = 2$ for dual-stream transmission. In order to consider both scenarios in the MCS search an estimate of the full MIMO channel matrix $\hat{\boldsymbol{H}}[k] \in \mathbb{C}^{N_{\mathrm{R}}\times N_{\mathrm{T}}}$ must be available at the receiver. With this estimate, the receiver calculates another effective channel matrix estimate $\hat{\boldsymbol{H}}'[k] = \hat{\boldsymbol{H}}[k]\boldsymbol{Q}[k]$,

with $\boldsymbol{Q}[k] \in \mathbb{C}^{N_{\mathrm{T}} \times N_{\mathrm{SS}}}$ denoting the precoding matrix. The corresponding post-processing SINRs, LQMs and estimated PERs are then obtained from $\hat{\boldsymbol{H}}'[k]$ for all possible supported precoding and MCS combinations. If $\hat{\boldsymbol{H}}[k]$ is not available, the channel is only known for the particular precoding mode. Hence, the performance of other combinations of precoding and MCS cannot be accurately estimated. A straightforward approach, which is also suggested in 802.11n [14, §20.3.13.3], is that the receiver selects an MCS based on the observed channel matrix only. That is, the MCS selection is based on a subset of the set of MCSs supported for the fully-known channel. This subset is determined by the observed signal dimension and the precoding capabilities of the considered MIMO system.

VIII. An Upper Bound for the Throughput of LAs

The common way of determining an upper bound for the throughput is to evaluate the ergodic capacity of the MIMO channel. However, the resulting bound is weak in this particular context and it cannot be achieved due to the following reasons: (i) we use only convolutional coding; (ii) we consider practical channel estimation; and (iii) the set Ω of candidate MCSs is not infinitely large in terms of available subcarrier modulation formats and code-rate combinations. Hence, we are interested in a practical bound on the throughput for any LA scheme. The genie-based method [2] provides such a bound. However the method has high complexity because it necessitates to simulate the PER for all MCSs, and large sets of SNRs and realizations of the channel transfer function. Instead we propose an upper bound and a low complexity algorithm to compute it. A similar bound was independently presented in [13]. We show below that it is not necessary to evaluate all candidate MCS $m \in \Omega$ as done in [13]. Instead, it suffices to evaluate an ordered subset of MCSs. The proposed bound can be seen as a further generalization of the bound in [31]. Notice that the algorithm in [31] generates a bound for a specific LA method, whereas the proposed algorithm generates a bound for any LA method.

We now describe the algorithm that computes an upper bound on the throughput for a given set of candidate MCSs. The algorithm - we coined it performance bound algorithm - is depicted in Fig. 6 for the sake of clarity. Define on Ω an ordering function h, such that $TP(h(i)) \geq TP(h(i-1)), i \in \{1, \cdots, |\Omega| - 1\}$. The bound is obtained as follows: first generate a realization of the channel transfer function and then obtain an index $i \leftarrow |\Omega| - 1$ with the corresponding MCS $m = h(i)$, *i.e.*, starting with the MCS having the largest throughput. In our case this MCS is 64QAM with $R_{\mathrm{c}} = 5/6$. This MCS is used to send a packet across the channel with the generated transfer function. If the transmission fails, *i.e.*, the packet is received incorrectly, the algorithm updates $i \leftarrow i-1$ (if $i \neq 0$) and obtain a new MCS $m = h(i)$. Notice that the throughput of the new MCS is equal or lower than that of the previous MCS. The new MCS is then used to send a packet across a channel with the same realization of the transfer function. These steps continue until the transmitted packet is received successfully or $i = 0$ which corresponds to the MCS with the lowest throughput. Information on the outcome of the last transmission (packet error event and throughput) is then saved for later evaluation. The algorithm then generates a new realization of the channel transfer function and starts a new cycle.

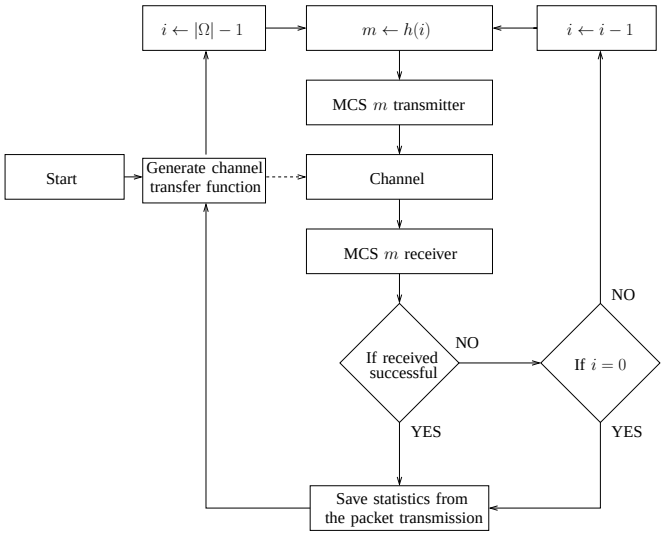

Fig. 6. Flow graph of the performance bound algorithm. The function h fulfils the property $TP(h(\Omega, i)) \geq TP(h(\Omega, i-1)), i \in \{1, \cdots, |\Omega| - 1\}$.

The upper bound is practically not achievable but it is tight enough to be of practical use as we will see in Section IX. The bound is derived in Appendix A and its tightness investigated in Appendix B.

IX. Numerical Results

For the evaluation of the FLA algorithm we utilize a simulator fully compliant with the IEEE 802.11n standard [14] and the IEEE channel models [16]. Channel estimation is performed based on the long training field provided in the preamble of a packet [14]. The channel estimates are smoothed before they are used in (4) for the computation of the post-processing SINR matrix $\boldsymbol{\Gamma}$. The correction parameters $\alpha(m), \beta(m), \kappa(m)$, and $\lambda(m)$ are found by means of preliminary simulations in which realizations of the channel transfer function are generated with both Channel Model B and Channel Model E (see Section IV-A). Table II reports the obtained values of these parameters. Only Channel Model B is used to obtain the results discussed below. The sequential search approach presented in Section VII is used to determine the MCS fed back to the transmitter.

A. Throughput and PER

Simulation results of the throughput and PER versus the SNR are shown in Fig. 7. The realizations of the channel response are normalized such that their time-averaged energy is unity. The SNR is defined as the inverse of the noise variance $\gamma = 1/\sigma_n^2$. For clarity we first discuss the results when FLA is not applied:

- The reported upper bound on the throughput is obtained using the performance bound algorithm described in Section VIII.

- Each curve indicated in dashed line "fixed MCS" represent the throughput or PER performance versus SNR of one individual MCS $m \in \Omega$.
- The reported "fixed MCS envelopes" are obtained for a given SNR by selecting the performance (throughput and PER) of the MCS achieving the maximum throughput at that SNR without considering any PER constraints. The bumpiness of the curve results due to the limited number of candidate MCSs, since a smooth transition in performance between the optimum MCSs for two consecutive SNR values is not always realized.
- The reported "PER-constraint envelopes" are obtained for a given SNR by selecting the performance (throughput and PER) of the MCS achieving the maximum throughput at each SNR, while maintaining a PER value less than 1%. These curves describe the performance of a slow link adaptation (SLA) method, which selects the MCS maximizing the throughput for a fixed noise variance, while maintaining a certain PER. Since the set of candidate MCSs is finite, the corresponding PER curve is also bumpy. The SLA method does not consider the instantaneous fading in the channel realizations and hence it is less effective than FLA, as we will see shortly.

The FLA algorithms under consideration operate as follows. Within each cycle a single data packet is sent with the MCS suggested by the receiver. The MCS feedback link is assumed to be free of error. The results are reported in Fig. 7. The throughput and PER values at each considered SNR value have been obtained by transmitting packets until 200 of them fail, with a maximum number of transmitted packets set to 3000.

It is observed that the throughput curves of the FLA algorithms using MMIBM, MIESM, EESM and RawBER are practically lying on top of each other, with a small degradation for EESM around $25\,\mathrm{dB}$ SNR. Using EESM and RawBER also yields a slightly larger PER than with MMIBM and MIESM. The throughput performance curves of MMIBM- and MIESM-based FLA methods are at most $1.7\,\mathrm{dB}$ shifted to the right of the throughput upper bound. Moreover, at a given throughput the SNR requirement for these FLA methods are $9.5\,\mathrm{dB}$ lower than for the PER-constraint envelope. The PER stabilizes around 1% within the SNR range $15-30\,\mathrm{dB}$. This feature, common to all four FLA methods investigated, is known as the inherently anti-fluctuating property of FLA [32].

All curves generated with the FLA algorithms approach the corresponding throughput value for the fixed MCSs $h(0)$ and $h(|\Omega|-1)$ at respectively low and high SNR regimes. An FLA algorithm is expected to have this behaviour. For sufficiently low SNR only MCS $h(0)$ may lead to error-free reception; at sufficiently high SNR, all MCS lead to successful packet reception, such that the FLA algorithm selects MCS $h(|\Omega|-1)$ to ensure the highest throughput.

If the channel is time-invariant, FLA is equivalent to SLA. This means that no gain is observed by using FLA compared to SLA in this case. On the other hand, if the channel has small time coherence, *i.e.*, the channel response changes fast, SLA will be ineffective due to the long averaging time. Generally, the smaller the time coherence, the higher the performance gain of FLA compared to SLA.

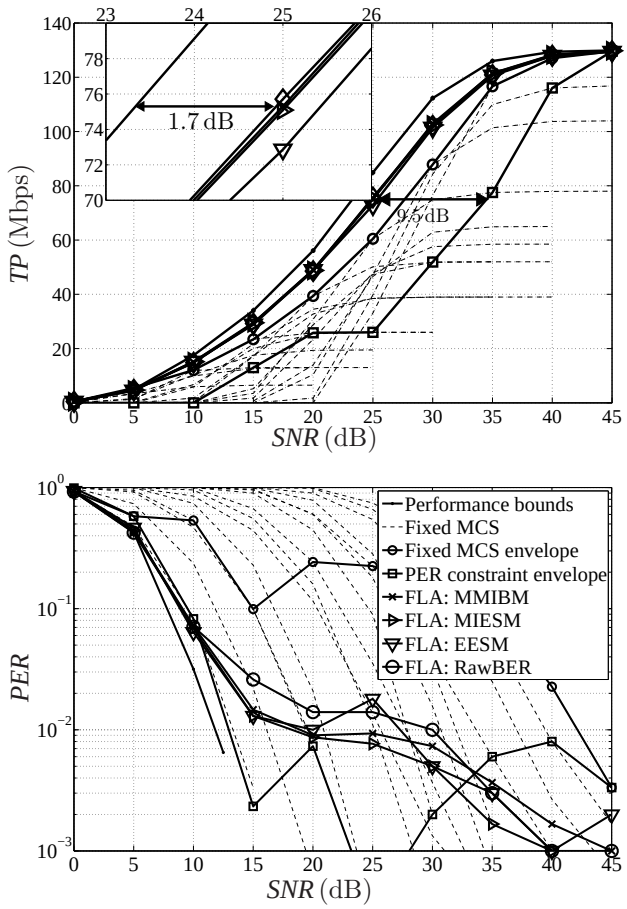

Fig. 7. Throughput (TP) and PER versus SNR of the considered schemes using the following settings: Channel Model B with bandwidth $20\,\mathrm{MHz}$, velocity of $1.2\,\mathrm{km/h}$, 2×2 MIMO OFDM system, $p = 1024\,\mathrm{Bytes}$ and $PER_{\mathrm{target}} = 1\%$ with $PER_{\mathrm{th}} = 3\%$ in (19).

B. MCS Feedback Delay

The performance of FLA is evaluated with respect to the MFB delay. The MFB delay is the time required for the MCS selected in the FLA algorithm to be effectively utilized at the transmitter. We consider only the MIESM-based FLA method to assess the impact of the MFB delay. The results for the other considered FLA methods are very similar as already observed in Fig. 7. Fig. 8 shows the throughput and PER versus the MFB delay. The throughput decreases and the PER increases as the MFB delay increases for both considered SNR levels of $20\,\mathrm{dB}$ and $30\,\mathrm{dB}$. At $4.5-5.5\,\mathrm{ms}$ MFB delay the loss in throughput is only minor but we observe a drastic degradation of the PER.

We also investigate the impact of scatter velocity on FLA. The results are shown in Fig. 9. Here we select a slightly larger $PER_{\mathrm{th}} = 5\%$. We further observe that for higher scatter velocity the observed PER increases faster as a function of the MFB delay.

In general, it is hard to know the MFB delay - in IEEE 802.11n it is unconstrained - or even the scatter velocity in advance. Both factors significantly impact the observed PER as shown in Fig. 8 and Fig. 9. To address this problem, the PER_{target} can be maintained by adjusting PER_{th} based on long-term PER statistics, without affecting the fast adaptation feature of FLA.

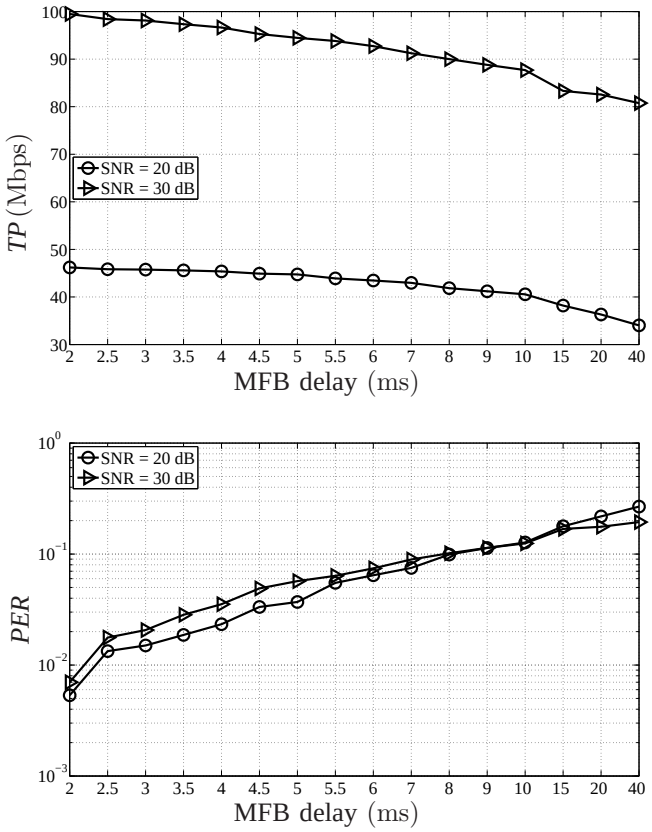

Fig. 8. Throughput (TP) and PER versus MFB delay of MIESM-based FLA with different scatter velocity using the following settings: Channel Model B with bandwidth $20\,\mathrm{MHz}$, velocity of $1.2\,\mathrm{km/h}$, 2×2 MIMO system, $p = 1024\,\mathrm{Bytes}$. The target PER of 1% is fulfilled up to an MFB delay of around $2.3\,\mathrm{ms}$. Note that the horizontal axes are non-linear.

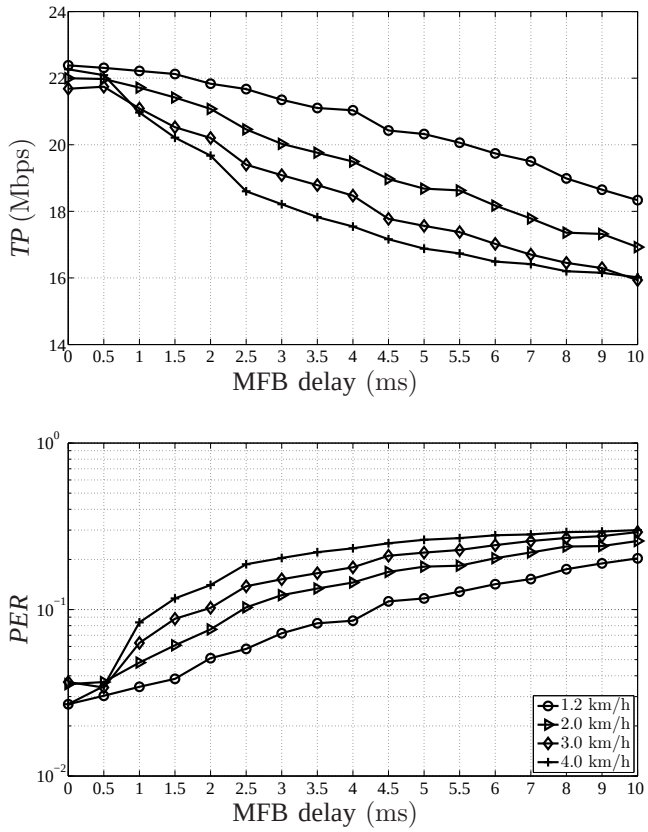

Fig. 9. Throughput (TP) and PER versus MFB delay of MIESM-based FLA with the velocity as parameter. Channel Model B with bandwidth $20\,\mathrm{MHz}$, 1×1 MIMO system, $SNR = 20\,\mathrm{dB}$, $p = 1024\,\mathrm{Bytes}$ and $PER_{\mathrm{th}} = 5\%$. Note that the horizontal axes are non-linear.

X. Conclusion

We have investigated four link quality metrics (LQMs), *i.e.*, the mean mutual information per coded bit mapping (MMIBM), the mutual information effective SNR mapping (MIESM), the effective SNR mapping (EESM) and the raw bit-error-rate (RawBER) for the purpose of fast link adaptation (FLA) in a multiple-input, multiple-output (MIMO) orthogonal frequency division multiplexing (OFDM) system operating in frequency selective channels. Our findings, exemplified for the IEEE 802.11n standard, indicate that introducing a correction parameter for MMIBM considerably improves the accuracy of the packet error rate (PER) estimation. The correction parameter depends on the modulation and coding scheme (MCS); but it is valid for a wide class of channel models. The PER estimators based on the modified MMIBM, MIESM, EESM and RawBER perform very closely. Furthermore, we proposed a practical algorithm to obtain an upper bound on the throughput of a link adaptation method using a given set of MCSs by means of simulations. The throughput that results from using the FLA algorithms is only $1.7\,\mathrm{dB}$ away from the throughput upper bound and shows a gain of up to $9.5\,\mathrm{dB}$ over a slow link adaptation (SLA) approach. FLA methods using MI metrics slightly outperform methods employing RawBER and EESM in terms of PER. FLA outperforms SLA in channels with low time coherence. The dependency on feedback delay was also investigated. We observed that the PER increases rapidly to an unacceptable level as the feedback delay increases. This effect may be counteracted by adjusting the PER threshold using an outer loop.

Acknowledgment

The authors would like to thank Dr. Karim Maouche from Wipro-NewLogic Technologies for kindly providing some of the simulation results.

Appendix

A. Derivation of the Upper Bound for the Throughput of Any LA

We show that the algorithm proposed in Section VIII yields an upper bound on the throughput. Let $\tilde{m} = f_{\mathrm{LA}}(\mathbf{H}, \gamma, \Omega) \in \Omega$ be the selection function of *any* LA algorithm for the channel $\mathbf{H} = [\boldsymbol{H}[k]]_{k=1,\ldots,N_{\mathrm{SD}}}$ and average SNR γ. The throughput of an LA algorithm can be written as

$$TP_{\mathrm{LA}}(\gamma, \Omega) = \mathbb{E}\Big\{ TP(\tilde{m})(1 - PER(\tilde{m}, \mathbf{H}, \gamma)) \Big\}, \qquad (21)$$

where $TP(\tilde{m})$ and $PER(\tilde{m}, \mathbf{H}, \gamma)$ are respectively the maximum throughput and the PER of MCS $\tilde{m}$ for the channel realization $\mathbf{H}$ and average SNR γ. Expectation is with respect to $\mathbf{H}$. The function TP_{LA} depends on Ω through

$\tilde{m} = f_{\mathrm{LA}}(\mathbf{H}, \gamma, \Omega)$. The throughput resulting from using the performance bound algorithm is

$$TP_{\mathrm{PBA}}(\gamma, \Omega) = \mathbb{E}\left\{ \sum_{m \in \Omega} TP(m) P_{\mathrm{s}}(m, \Omega, \mathbf{H}, \gamma) \right\} \quad (22)$$

with $P_{\mathrm{s}}(m, \Omega, \mathbf{H}, \gamma)$ denoting the probability that MCS m is selected by the algorithm from the set Ω for the channel realization $\mathbf{H}$ and γ. Although $\mathbf{H}$ is fixed, thermal noise casts the outcome of successful decoding as a probabilistic process. Consider now the partition $\Omega = \Omega_{\mathrm{high}} \cup \{\tilde{m}\} \cup \Omega_{\mathrm{low}}$. The set of MCSs with throughput higher than $TP(\tilde{m})$ is Ω_{high} and the set of MCSs with throughput lower than or equal to $TP(\tilde{m})$ is Ω_{low}. The evaluation of the algorithm on the set $\breve{\Omega} = \{\tilde{m}\} \cup \Omega_{\mathrm{low}}$ is

$$\begin{aligned} TP_{\mathrm{PBA}}(\gamma, \Omega) \geq TP_{\mathrm{PBA}}(\gamma, \breve{\Omega}) = \\ \mathbb{E}\Big\{ TP(\tilde{m}) P_{\mathrm{s}}(\tilde{m}, \breve{\Omega}, \mathbf{H}, \gamma) \Big\} + \\ \mathbb{E}\Big\{ \sum_{m \in \Omega_{\mathrm{low}}} TP(m) P_{\mathrm{s}}(m, \breve{\Omega}, \mathbf{H}, \gamma) \Big\}. \end{aligned} \quad (23)$$

Because the first evaluated MCS in the algorithm using the set $\breve{\Omega}$ is $\tilde{m}$, $P_{\mathrm{s}}(\tilde{m}, \breve{\Omega}, \mathbf{H}, \gamma) = (1 - PER(\tilde{m}, \mathbf{H}, \gamma))$. Hence the first term in (23) is the throughput of any LA algorithm as given in (21). Now,

$$TP_{\mathrm{PBA}}(\gamma, \Omega) \geq TP_{\mathrm{PBA}}(\gamma, \breve{\Omega}) \geq TP_{\mathrm{LA}}(\gamma, \Omega) \quad (24)$$

holds, because $TP(m) P_{\mathrm{s}}(m, \Omega, \mathbf{H}, \gamma) \geq 0$. Thus TP_{PBA} is an upper bound of throughput for *any* LA algorithm.

B. Discussion of the Tightness of the Upper Bound on the Throughput

Equality in (24) holds if $P_{\mathrm{s}}(\tilde{m}, \Omega, \mathbf{H}, \gamma) = 1$ and $P_{\mathrm{s}}(m, \Omega, \mathbf{H}, \gamma) = 0, \forall\, m \in \Omega_{\mathrm{high}} \cup \Omega_{\mathrm{low}}$. In this case the upper bound on the throughput can be achieved by an LA algorithm. If $PER \in \{0, 1\}$, then one MCS m will be selected with probability $P_{\mathrm{s}}(m, \Omega, \mathbf{H}, \gamma) = 1$ by the performance bound algorithm. This corresponds to a sharp transition from $PER(m, \mathbf{H}, \gamma) = 1$ to $PER(m, \mathbf{H}, \gamma + \epsilon) = 0$ with $\epsilon > 0$ in the PER-vs-SNR plot for all MCSs.

However, the PER is a smooth decreasing function of the SNR, which implies that, in general, more than one MCS m fulfill $P_{\mathrm{s}}(m, \Omega, \mathbf{H}, \gamma) > 0$ for a given $\mathbf{H}$ and γ. This gives contributions from the MCSs with larger and smaller throughputs relative to MCS $\tilde{m}$, and hence the upper bound is not reachable by *any* LA algorithm. So, the setup with the steepest PER-vs-SNR curve yields the tightest bound. We observe the following behaviours:

(i) For stronger codes, the PER curves drop faster versus SNR, leading to a tighter upper bound.

(ii) If only few MCSs exist with a high probability to be selected by the performance bound algorithm, *i.e.*, with high $P_{\mathrm{s}}(m, \Omega, \mathbf{H}, \gamma)$, then the bound will be tight. So, the more MCSs to choose from, the less tight the bound is. This can be concluded from the fact that the bound is reached at very low or high SNR where only one MCS is likely to be selected (see Fig. 7).

C. Approximations of the function $J(\cdot)$ in (7)

In [33], the function $J(\cdot)$ in (7) is approximated by

$$J(x) \approx \begin{cases} a_1 x^3 + b_1 x^2 + c_1 x, & 0 < x < 1.6363 \\ 1 - \exp(a_2 x^3 + b_2 x^2 + c_2 x + d_2), & 1.6363 \leq x < \infty \end{cases} \quad (25)$$

with the coefficients found for the MaxLog-demapper [20]

$$\begin{array}{lll} a_1 = -0.04210610 & b_1 = 0.209252 & c_1 = -0.00640081 \\ a_2 = 0.00181491 & b_2 = -0.142675 & c_2 = -0.08220540 \\ d_2 = 0.0549608. & & \end{array}$$

From (25) we obtain the inverse function of $J(x)$

$$J^{-1}(y) \approx \begin{cases} a_5 y^2 + b_5 y + c_5 \sqrt{y}, & 0 < y < 0.3646 \\ a_6 \log\left(b_6 (y - 1)\right) + c_6 y, & 0.3646 \leq y \leq 1 \end{cases} \quad (26)$$

with coefficients

$$\begin{array}{lll} a_5 = 1.09542 & b_5 = 0.214217 & c_5 = 2.33727 \\ a_6 = -0.706692 & b_6 = -0.386013 & c_6 = 1.75017\,. \end{array}$$

REFERENCES

[1] J. Cavers, "Variable-rate transmission for Rayleigh fading channels," *IEEE Trans. Commun.*, vol. 20, pp. 15–22, Feb. 1972.

[2] S. Simoens, S. Rouquette-Léveil, P. Sartori, Y. Blankenship, and B. Classon, "Error prediction for adaptive modulation and coding in multiple-antenna OFDM systems," *EURASIP Sig. Proc. J., Special Section: Advances in Signal Processing-assisted Cross-layer Designs*, vol. 86, no. 8, pp. 1911–1919, Aug. 2006.

[3] S. Hämäläinen, P. Slanina, M. Hartmann, A. Lappeteläinen, and H. Holma, "A novel interface between link and system level simulation," in *Proc. ACTS Mobile Summit*, Aalborg, Denmark, Oct. 1997, pp. 599–604.

[4] Member of IST-WINNER Consortium, "IST-2003-507581 WINNER, Deliverable 2.7, version 1.1, Assessment of Advanced Beamforming and MIMO Technologies," IST-WINNER, Tech. Rep., Feb. 2005.

[5] L. Berger, "Performance of Multi-Antenna Enhanced HSDPA," Ph.D. dissertation, Aalborg Universitet, Aalborg, Denmark, Jun. 2005.

[6] M. Lamarca and F. Rey, "Indicators for PER prediction in wireless systems: A comparative study," in *Proc. IEEE Veh. Techn. Conf. (VTC)*, vol. 2, no. 30, Stockholm, Sweden, May 2005, pp. 792–796.

[7] 3GPP TSG-RAN WG1, "System-level Evaluation of OFDM - Further Considerations," *R1-031303*, Nov. 2003.

[8] K. Sayana, J. Zhuang, and K. Stewart, "Link performance abstraction based on mean mutual information per bit (MMIB) of the LLR channel," *IEEE 802.16 BWA WG, C802.16m-07/097*, 2007.

[9] S. Shawn Tsai and Anthony C. K. Soong, "Effective-SNR Mapping for Modelling Frame Error Rates in Multiple-State Channels, C30-20030429-010," 3GPP2 - Ericsson, Tech. Rep., Apr. 2003, available at ftp://ftp.3gpp2.org/TSGC/Working/2003/2003-05-SanDiego/TSG-C-2003-05-San%20Diego/WG3/WG3%20Call,%202003.04.29/.

[10] M. Lampe, T. Giebel, H. Rohling, and W. Zirwas, "PER-prediction for PHY mode selection in OFDM communication systems," in *Proc. IEEE Global Telecomm. Conf. (GLOBECOM)*, San Francisco, CA, USA, Dec. 2003, pp. 25 – 29.

[11] T. L. Jensen, S. Kant, J. Wehinger, and B. Fleury, "Mutual information metrics for fast link adaptation in IEEE 802.11n," in *Proc. IEEE Int. Conf. on Comm. (ICC)*, Beijing, China, May 2008, pp. 4910–4915.

[12] P. H. Tan, Y. Wu, and S. Sun, "Link adaptation based on adaptive modulation and coding for multiple-antenna OFDM system," *IEEE J. Select. Areas Commun.*, vol. 26, no. 8, pp. 1599–1606, Oct. 2008.

[13] Y.-S. Choi and S. M. Alamouti, "A pragmatic PHY abstraction technique for link adaption and MIMO switching," *IEEE J. Select. Areas Commun.*, vol. 26, no. 6, pp. 960–971, Aug. 2008.

[14] IEEE Computer Society, "IEEE Standard 802.11n, Amendment 5: Enhancements for Higher Throughput," 2009.

[15] A. Paulraj, R. Nabar, and D. Gore, *Introduction to Space-Time Wireless Communications*. Cambridge University Press, 2003.

[16] Members of IEEE 802.11 TGn, "TGn Channel Models for IEEE 802.11 WLANs," *802.11-03/940r4*, May 2004.

[17] K. Brueninghaus, D. Astely, T. Salzer, S. Visuri, A. Alexiou, S. Karger, and G. Seraji, "Link performance models for system level simulations of broadband radio access systems," in *Proc. IEEE Int. Symp. on Personal, Indoor and Mob. Radio Comm. (PIMRC)*, Berlin, Germany, Sep. 2005, pp. 2306 – 2311.

[18] Y. Kim, J. Cioffi, and K. Holt, "Low complexity BICM-OFDM based MIMO receiver using successive interference cancellation," in *Proc. Wireless Tele. Symp. (WTS)*, Pomona, CA, USA, Apr. 2006, pp. 1–5.

[19] I. Land, P. Hoeher, and S. Gligorevic, "Computation of symbol-wise mutual information in transmission systems with LogAPP decoders and application to EXIT charts," in *Proc. 5th Int. ITG Conf. on Source and Channel Coding (SCC), Erlangen-Nuremberg, Germany*, Jan. 2004, pp. 195–202.

[20] T. L. Jensen and S. Kant, "Fast Link Adaptation for IEEE 802.11n," Master's thesis, Aalborg University, Denmark, Aug. 2007.

[21] B. A. Bjerke, J. Ketchum, R. Walton, S. Nanda, I. Medvedev, M. Wallace, and S. Howard, "Packet error probability prediction for system level simulations of MIMO-OFDM based 802.11n WLANs," in *Proc. IEEE Int. Conf. on Comm. (ICC)*, San Diego, CA, USA, May 2005, pp. 2538–2542.

[22] E. Westman, "Calibration and Evaluation of the Exponential Effective SINR Mapping (EESM) in 802.16," Master's thesis, KTH Electrical Engineering Dep., Stockholm, Sweden, Jul. 2006.

[23] Beijing University of Post and Telecommunications, "ESM Beta Training in 802.16e System 3.0," WiMAX Forum, AATG Report, 2007, Tech. Rep., 2007.

[24] Nortel Networks, "Modelling of Performance with Coloured Interference Using the EESM (Exponential Effective SIR Mapping)," 3GPP TSG RAN WG1 37, R1-040509, Tech. Rep., 2004.

[25] S. Nanda and K. Rege, "Frame error rates for convolutional codes on fading channels and concept of effective E_b/N_0," *IEEE Trans. Veh. Technol.*, vol. 47, no. 4, pp. 1245–1250, Nov. 1998.

[26] F. Peng, J. Zhang, and W. Ryan, "Adaptive modulation and coding for IEEE 802.11n," in *Proc. IEEE Wireless Comm. and Networking Conf. (WCNC)*, Hong Kong, China, Mar. 11-15, 2007, pp. 656 – 661.

[27] C. Stierstorfer and R. F. H. Fischer, "Adaptive interleaving for bit-interleaved coded modulation," in *Proc. 7th Int. ITG Conf. on Source and Channel Coding (SCC)*, Ulm, Germany, Jan. 2008.

[28] S. Lei and V. Lau, "Adaptive interleaving for OFDM in TDD systems," *IEE Proc. of Commun.*, vol. 148, pp. 77–80, Apr. 2001.

[29] S. Dolinar, D. Divsalar, and F. Pollara, "Code performance as a function of block size," TMO Progress Report 42-133, Tech. Rep., May 1998.

[30] R. C. Daniels, C. M. Caramanis, and R. W. Heath, "Adaption in convolutionally-coded MIMO-OFDM wireless systems through supervised learning and SNR ordering," *IEEE Trans. Veh. Technol.*, vol. 59, no. 1, pp. 114–126, Jan. 2010.

[31] K. Freudenthaler, A. Springer, and J. Wehinger, "Novel SINR-to-CQI mapping maximizing the throughput in HSDPA," in *Proc. IEEE Wireless Comm. and Networking Conf. (WCNC)*, Kowloon, China, 2007, pp. 2231–2235.

[32] M. Lampe, H. Rohling, and W. Zirwas, "Misunderstandings about link adaptation for frequency selective fading channels," in *Proc. IEEE Int. Symp. on Personal, Indoor and Mob. Radio Comm. (PIMRC)*, Lisbon, Portugal, Sep. 2002, pp. 710–714.

[33] S. ten Brink, G. Kramer, and A. Ashikhmin, "Design of low-density parity-check codes for modulation and detection," *IEEE Trans. Commun.*, vol. 52, no. 4, pp. 670–678, Apr. 2004.

Tobias Lindstrøm Jensen received his M.Sc. in Electrical Engineering from Aalborg University in 2007. In the same year, he was awarded the Computational Science in Imaging (CSI) Ph.D. fellowship from the Danish Research Council. Tobias L. Jensen is currently affiliated with the Deparment of Electronic Systems at Aalborg University. In 2007, he was a research associate at Wipro-NewLogic Technologies in Sophia-Antipolis, France. In 2009 he was a visiting researcher scholar at University of California, Los Angeles (UCLA). His current research interests include convex optimization based modelling, estimation and inverse problems.

Shashi Kant received M.Sc.E.E degree with specialisation in Signal and Information Processing in Communications from Aalborg University, Denmark, in August 2007. He was a research associate at Wipro NewLogic-Technologies, Sophia Antipolis, France from February 2007 to August 2007. From September 2007 to July 2008, he was a research assistant at Radio Access Technology Section, Department of Electronic Systems at Aalborg University and an external researcher at Nokia Siemens Networks, Aalborg, Denmark. Since July 2008, he has been with ST-Ericsson AT AB, LTE & 3G Modem Solutions (erstwhile Ericsson mobile platforms), Lund, Sweden, on 3GPP LTE physical layer algorithms development, simulation and performance evaluation. His interests are in the areas of time and frequency synchronization of OFDM systems and CQI estimation.

Joachim Wehinger was born in Hohenems, Austria, in 1975. He received his Dipl.-Ing. and Ph.D. degrees in electrical engineering from Technische Universität Wien, Austria, in 2001 and 2005 and an M.Sc. degree in digital communications from Chalmers Tekniska Högskola, Göteborg, Sweden in 2002, all with distinction. From 2001 to 2006 Dr. Wehinger was employed with Forschungszentrum Telekommunikation Wien (ftw.) where he was working as senior researcher and project manager in the area of multi-user receivers and smart antennas in 3G systems. During 2006-2007 Dr. Wehinger was with Wipro-NewLogic Technologies in Sophia-Antipolis, France, where he was in charge of modem development for IEEE 802.11n and Bluetooth 2.1+EDR. Since 2008 he has been employed as Senior Staff Engineer with Infineon Technologies in Munich, Germany, working on baseband-chip development for 3G+ mobile devices. He authored more than 30 papers in international journals and conferences and serves as reviewer for IEEE Trans. on Signal Processing, IEEE Trans. on Wireless Communications, and EURASIP Journal on Signal Processing. His interests are the area of low-complexity implementations, link adaptation, iterative receivers, MIMO, and multiuser communication systems.

Bernard H. Fleury received the diploma in electrical engineering and mathematics in 1978 and 1990 respectively, and the doctoral degree in electrical engineering in 1990 from the Swiss Federal Institute of Technology Zurich (ETHZ), Switzerland.

Since 1997 Bernard H. Fleury has been with the Department of Electronic Systems, Aalborg University, Denmark, as a Professor in Communication Theory. He is the Head of the Section Navigation and Communications, one of the eight labs of this department. From 2006 to 2009 he was affiliated as a Key Researcher with FTW Forschungszentrum Telekommunikation Wien, Austria. In 1999 he was elected IEEE Senior Member. During 1978-85 and 1992-96 he was a Teaching Assistant and a Senior Research Associate respectively at the Communication Technology Laboratory at ETHZ. Between 1988 and 1992 he was a Research Assistant at the Statistical Seminar at ETHZ.

Prof. Fleury's general fields of interest cover numerous aspects within communication theory and signal processing, mainly for wireless communications. His current areas of research include stochastic modelling and estimation of the radio channel, especially for multiple-input multiple-output (MIMO) applications and in fast time-varying environments, iterative message-passing processing with focus on the design of efficient, feasible advanced receiver architectures, and localization in wireless terrestrial systems. He has authored and co-authored more than 100 publications in these areas. Prof. Fleury has developed with his staff a high-resolution method for the estimation of radio channel parameters that has found a wide application and has inspired similar estimation techniques both in academia and in industry.